Nucleic Acids Research, 2018 **1**
doi: 10.1093/nar/gky774

Repair protein persistence at DNA lesions characterizes XPF defect with Cockayne syndrome features

Mariangela Sabatella[1,2], Arjan F. Theil[1,2], Cristina Ribeiro-Silva[1,2], Jana Slyskova[1,2], Karen Thijssen[1,2], Chantal Voskamp[1], Hannes Lans[1,2,*] and Wim Vermeulen[1,2,*]

[1]Department of Molecular Genetics, Erasmus MC, University Erasmus Medical Center Rotterdam, 3000 CA, The Netherlands and [2]Oncode Institute, Erasmus MC, University Erasmus Medical Center Rotterdam, 3000 CA, The Netherlands

Received March 29, 2018; Revised July 19, 2018; Editorial Decision August 14, 2018; Accepted August 16, 2018

ABSTRACT

The structure-specific ERCC1-XPF endonuclease plays a key role in DNA damage excision by nucleotide excision repair (NER) and interstrand crosslink repair. Mutations in this complex can either cause xeroderma pigmentosum (XP) or XP combined with Cockayne syndrome (XPCS-complex) or Fanconi anemia. However, most patients carry compound heterozygous mutations, which confounds the dissection of the phenotypic consequences for each of the identified *XPF* alleles. Here, we analyzed the functional impact of individual pathogenic *XPF* alleles on NER. We show that XP-causing mutations diminish XPF recruitment to DNA damage and only mildly affect global genome NER. In contrast, an XPCS-complex-specific mutation causes persistent recruitment of XPF and the upstream core NER machinery to DNA damage and severely impairs both global genome and transcription-coupled NER. Remarkably, persistence of NER factors at DNA damage appears to be a common feature of XPCS-complex cells, suggesting that this could be a determining factor contributing to the development of additional developmental and/or neurodegenerative features in XP patients.

INTRODUCTION

Xeroderma pigmentosum (XP) and Cockayne syndrome (CS) are rare autosomal recessive photosensitive disorders caused by mutations in genes that encode factors involved in nucleotide excision repair (NER). XP patients display pigmentation abnormalities, a >2000-fold increased risk of skin cancer and over 20% of the patients develop progressive neurodegeneration (1). CS patients display severe growth failure, progressive neurodegeneration and segmental progeria but do not develop cancer (2). XP patients are classified in complementation groups XP-A to XP-G and the variant XP-V, according to the mutated gene, while CS is caused by mutations in the *CSA* and *CSB* genes. Intriguingly, some patients from complementation groups XP-B, XP-D, XP-G and XP-F combine dermatological features of XP with developmental and progressive neurodegenerative features of CS, representing the rare *Xeroderma pigmentosum*-Cockayne syndrome (XPCS) complex (3,4). Also, patients from complementation group XP-A can exhibit XP combined with severe growth failure and progressive neurodegeneration, which is often referred to as De Sanctis Cacchione (DSC) syndrome (5). The type of disease and severity of symptoms are thought to depend on which gene is mutated and to which extent NER is affected, but it is not properly understood how mutations in the same genes can cause different diseases.

NER is a major DNA repair pathway responsible for removing UV light induced cyclobutane-pyrimidine dimers (CPDs) and 6-4 pyrimidine-pyrimidone photoproducts (6-4PPs) and other bulky lesions such as intrastrand crosslinks and ROS-induced cyclopurines (6,7). DNA damage is detected by two sub-pathways: global genome-NER (GG-NER), which detects damage located anywhere in the genome by the concerted action of the UV-DDB/XPE and XPC-RAD23B-CETN2 complex, and transcription coupled-NER (TC-NER), which detects damage in the template strand of transcribed genes through stalling of RNA polymerase II and subsequent recruitment of the CSA (ERCC8), CSB (ERCC6) and UVSSA proteins. Damage detection by either sub-pathway leads to recruitment of the basal transcription factor complex IIH (TFIIH). TFIIH opens the DNA helix and verifies the presence of DNA le-

*To whom correspondence should be addressed. Tel: +31 10 7038169; Email: w.lans@erasmusmc.nl
Correspondence may also be addressed to Wim Vermeulen. Email: w.vermeulen@erasmusmc.nl
Present address: Chantal Voskamp, Department of Orthopaedics, Erasmus MC, Rotterdam 3015 CN, The Netherlands.

sions using its XPB (ERCC3) ATPase and the 5′–3′ helicase activity of its XPD (ERCC2) subunit, which is stimulated by the single strand DNA damage binding protein XPA. XPA binds damaged DNA and interacts with multiple NER factors and is therefore considered a central NER organizer. Together with RPA, XPA facilitates the recruitment and correct positioning of the two structure-specific endonucleases, ERCC1-XPF (XPF is also known as ERCC4) and XPG (ERCC5), that incise the damaged strand respectively 5′ and 3′ to the lesion. The resulting 22–30 nt gap is then repaired by DNA synthesis and sealed by ligation.

ERCC1-XPF is an obligate dimer that binds to XPA via its ERCC1 subunit and incises double stranded DNA 5′ to a stretch of single stranded DNA using the catalytic activity of the highly conserved nuclease domain in XPF (8–11). Besides NER, ERCC1-XPF nuclease activity is also implicated in removing 3′ overhangs during some forms of double strand break repair and is critical in unhooking interstrand crosslinks (ICLs) as part of the Fanconi anemia (FA) repair pathway (12,13). Defects in this latter repair pathway lead to the rare disease FA, which is characterized by congenital growth abnormalities, bone marrow failure and increased susceptibility to cancer (14). Mutations in *ERCC1-XPF* have been found in patients exhibiting a range of phenotypically pleiotropic diseases including XP, CS, XPCS and FA, but also the more severe cerebro-oculo-facio-skeletal syndrome and XPF–ERCC1 progeroid syndrome (11,15–18).

The difference in severity of symptoms associated with ERCC1-XPF defects have been attributed to differences in mislocalization of the complex to the cytoplasm, which is observed in many XP-F group patient fibroblasts (19). There exists wide consensus that XP symptoms are specifically caused by defects in GG-NER (1) and FA symptoms by defects in ICL repair (ICLR) (14,20). Thus, mutations that impair the activity of ERCC1-XPF in either GG-NER or ICLR will give rise to XP or FA, respectively. The exact etiology of CS is, however, debated and opinions vary as to whether CS symptoms are primarily caused by defects in TC-NER or whether defects in other DNA repair pathways, transcription, stress responses and/or mitochondria may play a role as well (6,21–23). It is therefore not understood why certain mutations in ERCC1-XPF only give rise to XP or FA whereas others in addition cause CS features. Moreover, in most patients, mutations are present as compound heterozygous and different mutation combinations are associated with different diseases (Table 1), convoluting a clear understanding of the contribution of each mutation to the disease phenotype.

To clarify the molecular mechanism that gives rise to XPCS, we investigated how specific XPF mutations found in patients affected with XP, XPCS or FA impair the activity of the ERCC1-XPF complex in response to DNA damage induction by UV irradiation. We show that XPF with an XP mutation is inefficiently recruited into the NER machinery but retains repair activity. Conversely, XPCS mutant XPF persists at sites of DNA damage and hardly displays repair activity, leading to continuous recruitment of the core NER machinery.

MATERIALS AND METHODS

Cell culture, generation of cell lines and cloning of XPF-GFP constructs

U2OS cell lines were cultured in a 1:1 mixture of DMEM and F10 supplemented with 10% fetal calf serum (FCS) and 1% penicillin-streptomycin (PS) at 37°C and 5% CO_2. Wild type hTERT immortalized C5RO and patient fibroblasts XPCS1CD, CS1USAU (15), hTERT immortalized XP42RO (24), XP32BR (19), XP6BE (25), hTERT immortalized XPCS1RO (26), XPCS2 (27), XPCS1BA (28) and XP25RO (29) were cultured in F10 supplemented with 15% FCS and 1% PS at 37°C and 5% CO_2. To generate U2OS XPF KO cells, U2OS cells were simultaneously transfected with pLentiCRISPR-V2 plasmids (30) containing an sgRNA targeting exon 1 (TGGAACT GCTCGACACTGAC) and an sgRNA targeting exon 2 (CGCTATGAAGTTTACACACA) of XPF. Following selection with puromycin, single XPF KO clones were analyzed by immunoblot and sequencing. Tracking Indels by Decomposition analysis was performed as described in Brinkman *et al.* (31). To generate GFP-tagged wild type XPF (XPF-wt), full length XPF cDNA, kindly provided by Orlando D. Schärer, was fused to GFP at its C-terminus and cloned into pLenti-CMV-Blast-DEST (32). GFP-tagged XPF mutants were generated by site directed mutagenesis using primers listed in Supplementary Table S1 and cloned into pLenti-CMV-Blast-DEST or pLenti-CMV-Puro-DEST. GFP-tagged wild type and mutant XPF were introduced in U2OS XPF KO cells by lentiviral transduction and cells were selected using blasticidin or puromycin. Cloning details are available upon request.

Clonogenic survival assays

To determine UV and mitomycin C (MMC) sensitivity, 500 cells were seeded in triplicate in six-well plates. 24 h after seeding, cells were irradiated with UV (0, 0.5, 1, 2, 4 J/m^2; 254 nm UV-C lamp, Philips) or treated with MMC (0, 0.3, 0.6, 0.9, 1.2, 1.5 μg/ml; Sigma). After 5–7 days, cells were fixed and stained with 50% methanol, 7% acetic acid, 0.1% Brilliant Blue R (Sigma) and counted using the integrated colony counter GelCount (Oxford Optronix). The number of colonies after treatment was normalized to the number in non-treated conditions and plotted as average survival percentage of three independent experiments. Statistical difference was calculated using a paired two-tailed Student's *t*-test.

Live cell imaging and fluorescence recovery after photobleaching (FRAP)

For live cell imaging, cells were seeded on coverslips and imaged with a Leica TCS SP5 confocal microscope using a 63x/1.4 NA HCX PL APO CS oil immersion lens (Leica Microsystems) at 37°C and 5% CO_2. FRAP was performed as previously described (33). Briefly, fluorescence was imaged within a strip of 512 × 16 pixels stretched over the width of the nucleus (zoom 9×) at 1400 Hz every 22 ms using 488 nm laser at low power until steady-state levels were reached. Next, fluorescence signal was bleached using high

Table 1. Features of studied XPF mutations

Amino acid change	Nucleotide change	Compound heterozygous with	Cell line	Disease[a]	UV sensitivity[b]	MMC sensitivity[b]	UDS[c]	RRS[c]	Reference
C236R	706T > C	R589W	XPCS1CD	XPCS + FA features	+	+	8%	24%	(15)
		Y577*	CS1USAU	XPCS	+	-	10%	16%	(15)
P379S	1135C > T	R589W	XP32BR	mild XP	+	ND	10–16%	ND	(19,39)
			XP72BR	mild XP		ND	36%	ND	(39)
		silent allele	XP7NE	mild XP	+	ND	30%	ND	(19)
R589W	1765C > T	P379S	XP32BR	mild XP	+	ND	10–16%	ND	(15,39)
		R799W	XP24BR	severe XP, neurodegeneration	+	ND	4–5%	ND	(15,19,39)
		del exon 3	AS871	severe XP, neurodegeneration	+	ND	15%	ND	(15,19)
		C236R	XPCS1CD	XPCS + FA features	+	+	8%	24%	(15)
R689S	2065C > A	T495Nfs*6	FA104	FA	-	+	ND	ND	(16)
D715A	2144A > C				ND	ND	ND	ND	(8)
S786F	2357C > T				-	+	ND	ND	(40)

[a]XP: xeroderma pigmentosum; CS: Cockayne syndrome; XPCS: xeroderma pigmentosum-Cockayne syndrome; FA: Fanconi anemia.
[b]+ hypersensitive to either UV or MMC; - not hypersensitive; ND, not determined.
[c]RRS and UDS levels in XPCS1CD and CS1USAU were estimated based on graphs in Figure 1C and D of (15).

laser power (100%) and recovery of the signal was measured at low laser power every 22 ms until steady-state levels were reached. To perform FRAP on local UV damaged areas (Figure 3D), the entire nucleus of each cell was imaged at 400 Hz every 648 ms using low laser power. Fluorescence signal within a small region (1.5 μm × 1.5 μm) stretched over the local damage area was bleached with high laser power and recovery of the fluorescence in time was measured at low laser power every 648 ms. Fluorescence signals were normalized to the average fluorescence intensity before bleaching and bleach depth. The immobile fraction (F_{imm}) (Figure 3C) was determined using the fluorescence intensity measured immediately after bleaching (I_0), and the average steady-state fluorescence level once recovery was complete, from untreated cells ($I_{final,\,unt}$) and UV- treated cells ($I_{final,\,UV}$) and applying the formula: $F_{imm} = 1 - (I_{final,UV} - I_{0,UV})/(I_{final,unt} - I_{0,uv})$ (34). Statistical difference was calculated using an unpaired two-tailed Student's *t*-test. LAS AF software (Leica) was used for imaging and quantification.

Immunofluorescence

To perform immunofluorescence experiments, cells were seeded on coverslips and, when indicated, irradiated with 60 J/m^2 (254 nm UVC lamp, Philips) through an 8 μm microporous filter (Millipore) to inflict local DNA damage. To determine CPD removal, cells were globally irradiated with 10 J/m^2. Cells were fixed at the indicated time points with 2% paraformaldehyde and 0.1%Triton X-100 and permeabilized for 20 min using 0.1% Triton X-100 in PBS. To visualize CPDs, cells were incubated with 0.07 M NaOH in PBS for 5 min to denature DNA. Cells were then washed with PBS containing 0.15% glycine and 0.5% BSA and incubated with primary antibodies for 2 h. After thorough washing with PBS containing 0.1% Triton X-100, cells were incubated with Alexa Fluor conjugated secondary antibodies (488, 555 and 633; Invitrogen) for 1 h. Coverslips were mounted using DAPI Vectashield (Vector Laboratories) and imaged using an LSM700 microscope equipped with a 40x Plan-apochromat 1.3 NA oil immersion lens (Carl Zeiss). Quantification of repair protein recruitment or CPD signal was performed using FIJI image analysis software. Statistical difference was calculated using an unpaired two-tailed Student's *t*-test. Primary antibodies used were against XPF (sc-136153, Santa Cruz Biotechnology), XPC (homemade fraction 5 or A301-121A, Bethyl), ERCC1 (ab129267, Abcam), GFP (ab290, Abcam), CPD (TDM-2; Cosmobio), XPB (sc-293, Santa Cruz), XPD (ab54676, Abcam), XPG (A301-484A, Bethyl) and XPA (sc-853, Santa Cruz Biotechnology).

Cell fractionation

For cell fractionation, cells were irradiated with 5 J/m^2 UVC (254 nm lamp, Philips) or left untreated. Cells were collected by trypsinization, washed and incubated in HEPES Buffer (30 mM HEPES pH 7.5, 130 mM NaCl, 1mM $MgCl_2$, 0.5% triton X-100 and protease inhibitors) on ice for 30 min. Samples were centrifuged at 15 000g for 20 min and separated into supernatant (soluble fraction) and pellet (chromatin fraction), which was solubilized by treatment with 250 U of benzonase (Merck Millipore). Both fractions were analyzed by immunoblot. Statistical difference was calculated using a paired two-tailed Student's *t*-test.

Immunoblot

For immunoblot analysis, cells or samples were collected in 2× sample buffer (125 mM Tris–HCl pH 6.8, 20% glycerol, 10% 2-β-mercaptoethanol, 4% SDS, 0.01% Bromophenol Blue) and boiled at 98°C for 5 min. Protein lysate was separated by SDS-PAGE and transferred to a PVDF membrane

(0.45 μm, Merck Millipore). Membranes were blocked in 2% BSA and incubated with primary and secondary antibodies for 2 h or overnight. Antibodies used were against XPF (sc-136153, Santa Cruz), ERCC1 (sc-17809, Santa Cruz), CSB (sc-10459, Santa Cruz), H2B (sc-8650, Santa Cruz) and Ku-70 (sc-17789, Santa Cruz Biotechnology). Secondary antibodies were conjugated with CF IRDye 680 or 770 (Sigma) and visualized using the Odyssey CLx Infrared Imaging System (LI-COR Biosciences).

Recovery of RNA synthesis

RRS was performed as described (35). Briefly, cells were mock treated or irradiated with 6 J/m^2 UVC (254 nm lamp, Philips) and RNA was labeled 24 h later by incubation with EU for 1 h. Cells were fixed in 4% paraformaldehyde and permeabilized with 0.1% Triton X-100 in PBS. To visualize EU incorporation, cells were incubated in Click-it buffer containing Atto 594 Azide (60 μM, Atto Tec.), Tris-HCl (50 mM, pH 7.6), CuSO4.5H_2O (4 mM, Sigma) and ascorbic acid (10 mM, Sigma) for 1 h and then washed with PBS containing 0.1% Triton X-100. DAPI (Sigma) was used to stain DNA and slides were mounted using Aqua-Poly/Mount (Polysciences, Inc.). Images were acquired using an LSM700 confocal microscope equipped with a 40× Plan-apochromat 1.3 NA oil immersion lens (Carl Zeiss Micro Imaging Inc.). RRS levels were quantified by averaging the total nuclear fluorescence intensities of at least 100 cells per experiment with FIJI image analysis software and normalization to fluorescence levels in control conditions.

Unscheduled DNA synthesis

UDS was measured in local UV damaged areas within cells after irradiation with 60 J/m^2 (254 nm UVC lamp, Philips) through an 8 μm microporous filter (Millipore). Cells were incubated with EdU for 30 min or 1 h, pre-extracted with PBS containing 0.1% Triton X-100 and fixed with 2% paraformaldehyde in PBS. Next, cells were permeabilized using PBS containing 0.1% Triton X-100 for 10 min and blocked in PBS containing 1.5% BSA for 10 min. To visualize CPDs, DNA was denatured with 0.07 M NaOH for 5 min. To visualize EdU incorporation, cells were incubated in Click-it buffer containing Atto 594 Azide (60 μM, Atto Tec.), Tris–HCl (50 mM, pH 7.6), CuSO4*5H2O (4 mM, Sigma) and ascorbic acid (10 mM, Sigma) for 1 h and then washed with PBS containing 0.1% Triton X-100. Subsequently, cells were washed with PBS containing 0.15% glycine and 0.5% BSA and incubated with GFP (ab290, Abcam) and CPD (TDM-2; Cosmobio) antibodies for 2 h. After washing with PBS containing 0.1% Triton X-100 and PBS, cells were incubated with Alexa Fluor conjugated secondary antibodies (488 and 633; Invitrogen) for 1 h. Coverslips were mounted using DAPI Vectashield (Vector Laboratories) and imaged using an LSM700 microscope and 40× Plan-apochromat 1.3 NA oil immersion lens (Carl Zeiss). The fluorescent EdU signal at local sites of damage from at least 60 cells per condition was quantified using FIJI image analysis and averaged. Statistical difference was calculated using an unpaired two-tailed Student's *t*-test.

RESULTS

Generation of *XPF* knockout and XPF-GFP expressing cells

To study how *XPF* deficiency can lead to different diseases, we determined how *XPF* mutations found in XP, XPCS and FA patients affect the spatio-temporal response of the ERCC1-XPF complex to DNA damage. To this end, we first generated an XPF knockout (KO) cell line, to be able to compare different mutant XPF proteins, which in patients most often occur as compound heterozygous, in the same genetic background. Following transfection of U2OS cells with plasmids expressing Cas9 and sgRNAs targeting exon 1 and exon 2 of *XPF*, we selected an *XPF* KO clone carrying multiple indel mutations in both exons predicted to lead to early truncation of the protein, as revealed by sequencing and tracking indels by decomposition analysis (31) (Supplementary Figure S1). In this clone, XPF was not detectable by immunoblot nor by immunofluorescence (Figure 1A-B). To functionally confirm the absence of XPF, we determined protein levels of ERCC1, whose stability depends on the presence of XPF (36,37), and found these to be strongly reduced in the XPF KO cells (Figure 1A). Moreover, extreme hypersensitivity to UV (Figure 1C), which generates lesions that are substrates for NER, and to Mitomycin C (MMC; Figure 1D), which in addition induces ICLs, confirmed that these KO cells lack XPF activity and are therefore completely NER- and ICLR-deficient. Next, we stably expressed GFP-tagged wild type XPF (XPF-wt) in the XPF KO cells, which rescued UV and MMC hypersensitivity and stabilized protein levels of ERCC1 (Figure 1A, C and D). To further validate the functionality of XPF-wt, we applied UVC irradiation through a microporous filter to inflict local DNA damage within the nuclei of the cells (38). XPF-wt clearly accumulated at sites of local UV damage (LUD) marked by XPC, in cells fixed 30 min after irradiation, similarly to endogenous XPF in control U2OS cells (Figure 1B). Together, these data indicate that repair deficient XPF KO cells can be fully complemented by GFP-tagged wild type XPF.

XP, XPCS and FA mutations differently affect UV and MMC sensitivity

Next, we stably expressed GFP-tagged XPF mutants mimicking alleles previously reported in patients affected with XP, XPCS and FA in the XPF KO cells (Table 1 and Figure 2A). We introduced two amino acid substitutions in the helicase-like domain of XPF: P379S (XPF-P379S), found in patients affected with mild XP (39) and C236R (XPF-C236R), found in XPCS patients (15). We also introduced the R589W substitution (XPF-R589W), found as compound heterozygous together with P379S in mild XP but together with C236R in XPCS with FA features (15,19,39). Furthermore, we generated nuclease domain substitution mutants R689S (XPF-R689S), found in an XPF FA patient (16) and S786F (XPF-S786F), which was reported to disrupt ICLR but not NER (40). As control, we generated a nuclease-dead mutant unable to cleave DNA, by introducing the D715A substitution (XPF-D715A) (8).

Live cell imaging and immunofluorescence showed that all XPF mutants, except XPF-R589W, localized exclusively

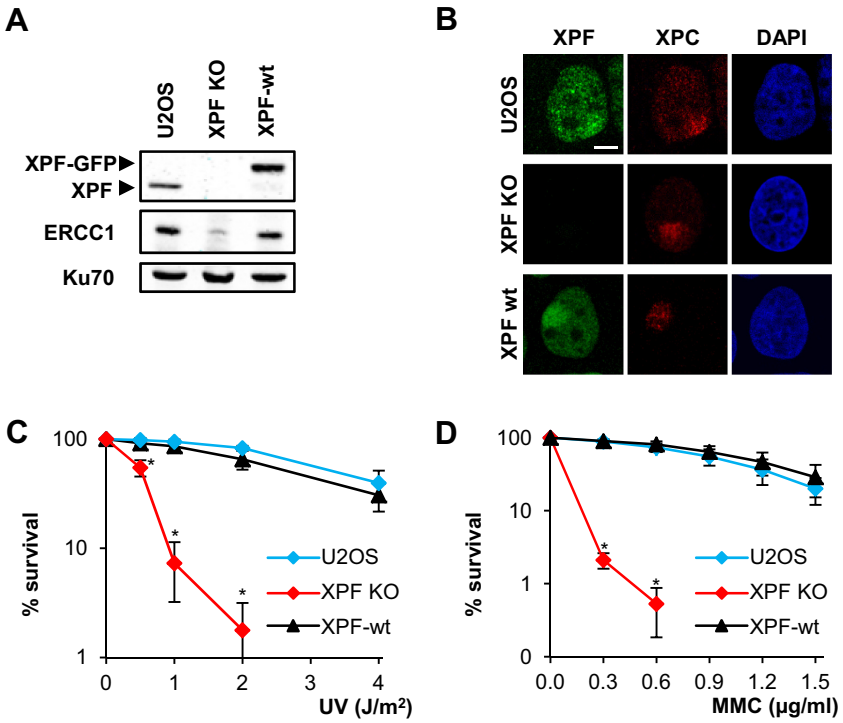

Figure 1. Generation of *XPF* knockout and XPF-GFP expressing cells. (**A**) Immunoblot showing XPF and ERCC1 expression in U2OS, XPF knockout (KO) and XPF-GFP (XPF-wt) expressing XPF KO cells. Ku70 staining is shown as loading control. (**B**) Immunofluorescence pictures showing localization of endogenous XPF in U2OS (top panel) and XPF-wt in XPF KO cells (bottom panel) to LUD induced by 60 J/m^2 UVC irradiation through an 8 μm microporous filter. Cells were fixed 30 minutes after UV and stained against XPF and XPC, to mark sites of local damage. Scale bar: 5 μm. (**C**) Clonogenic UV survival assays of U2OS, XPF KO and XPF-wt expressing XPF KO cells. (**D**) Clonogenic MMC survival assays of U2OS, XPF KO and XPF-wt expressing XPF KO cells. Survival assays are plotted as average of three independent experiments, each performed in triplicate. Error bars represent the SEM. Statistical significant difference ($P < 0.05$) compared to U2OS for each dose is indicated by *.

in the nucleus (Figure 2B-C). ERCC1 is stabilized by its interaction with XPF and translocates to the nucleus only when in complex with nuclear XPF (19,36,37,41). Noticeably, in all cell lines expressing XPF mutants, except in the cell line expressing the R589W mutant, ERCC1 protein levels were increased (Supplementary Figure S1B; compare with XPF KO in Figure 1A) and ERCC1 was clearly localized in the nucleus compared to XPF KO (Figure 2C). These results indicate that these XPF mutants interact normally with ERCC1, which was previously also shown for C236R, R689S and D715A XPF mutants (8,15,16). The only exception was XPF-R589W, which showed predominant or exclusive localization in the cytoplasm in ∼54% of cells and equal localization in cytoplasm and nucleus in ∼44% of cells (Figure 2B). Although this mutant appeared to stabilize ERCC1 levels on immunoblot (Supplementary Figure S1B), in immunofluorescence no clearly increased ERCC1 levels were observed, not even when XPF was also partially localized in the nucleus (Figure 2C). To determine the impact of each separate mutation on the different functions of XPF in NER and ICLR, we measured sensitivity of each cell line to UV irradiation and MMC. This showed that cells expressing the C236R, R589W and D715A XPF mutants were strongly hypersensitive to UV (Figure 2D), but cells expressing the P379S, R689S and S786F XPF mutants only showed mild to hardly any UV sensitivity. Cells expressing the C236R, R589W and D715A XPF mutants were also strongly hypersensitive to MMC, while cells expressing XPF-P379S were not sensitive to MMC (Figure 2E). However, contrarily to their mild UV survival, cells expressing XPF-R689S and XPF-S786F were hypersensitive to MMC. These data indicate that XPF mutations found in mild XP and FA patients, i.e. P379S and R689S, and the ICLR-defective S786F mutation, do not fully compromise the ability of XPF to function in NER. R689S and S786F nonetheless do impair XPF function in ICLR. The C236R mutation found in XPCS patients, of which one has features of FA, impedes XPF function in NER and possibly also in ICLR, but this latter is difficult to judge because mild MMC sensitivity can also be caused by a NER defect (17,42). Strikingly, XPF-R589W was unable to complement both NER and ICLR, similar as nuclease-dead XPF-D715A. We therefore conclude that R589W, which causes XPF to localize in the cytoplasm and is only found in compound heterozygous combinations in patients (Table 1) (15,19,39), is a functional null mutation.

Impaired recruitment of XPF-P379S contrasts persistent recruitment of XPF-C236R

To better understand the activity of each XPF mutant in NER, we determined LUD recruitment of the mutants at multiple time points after UV irradiation through a microporous filter using immunofluorescence. LUD was visualized using CPD staining, which is commonly used as

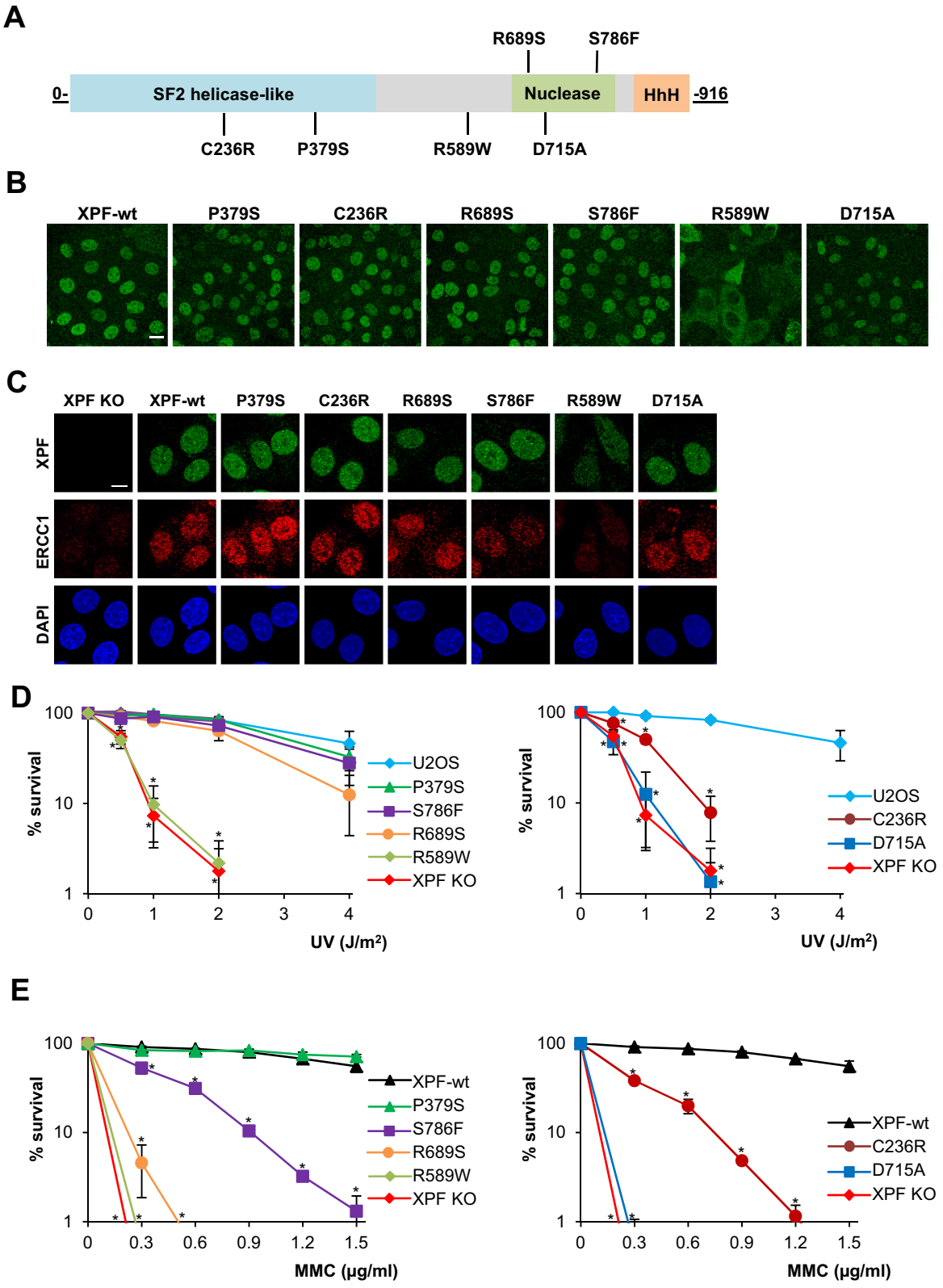

Figure 2. Expression of XPF mutants and sensitivity to UV and MMC. (**A**) Schematic representation of the XPF protein and annotation of the amino acid substitutions studied in this paper. (**B**) Live cell images showing the subcellular distribution of GFP-tagged XPF-wt and XPF mutants stably expressed in U2OS XPF KO cells. Scale bar: 20 μm. (**C**) Immunofluorescence images showing the subcellular distribution of GFP-tagged XPF-wt and XPF mutants stably expressed in XPF KO cells, together with ERCC1 expression visualized by staining with an antibody against ERCC1. Scale bar: 10 μm. (**D,E**) Clonogenic survival assays showing the sensitivity to UV (D) and MMC (E) treatment of XPF KO cells expressing XPF mutants compared to U2OS, XPF KO only and XPF-wt expressing cells. Results are plotted as average of three (UV) or two (MMC) independent experiments, each performed in triplicate. Error bars represent the SEM. Statistical significant difference ($P < 0.05$) compared to U2OS or XPF-wt for each dose is indicated by *.

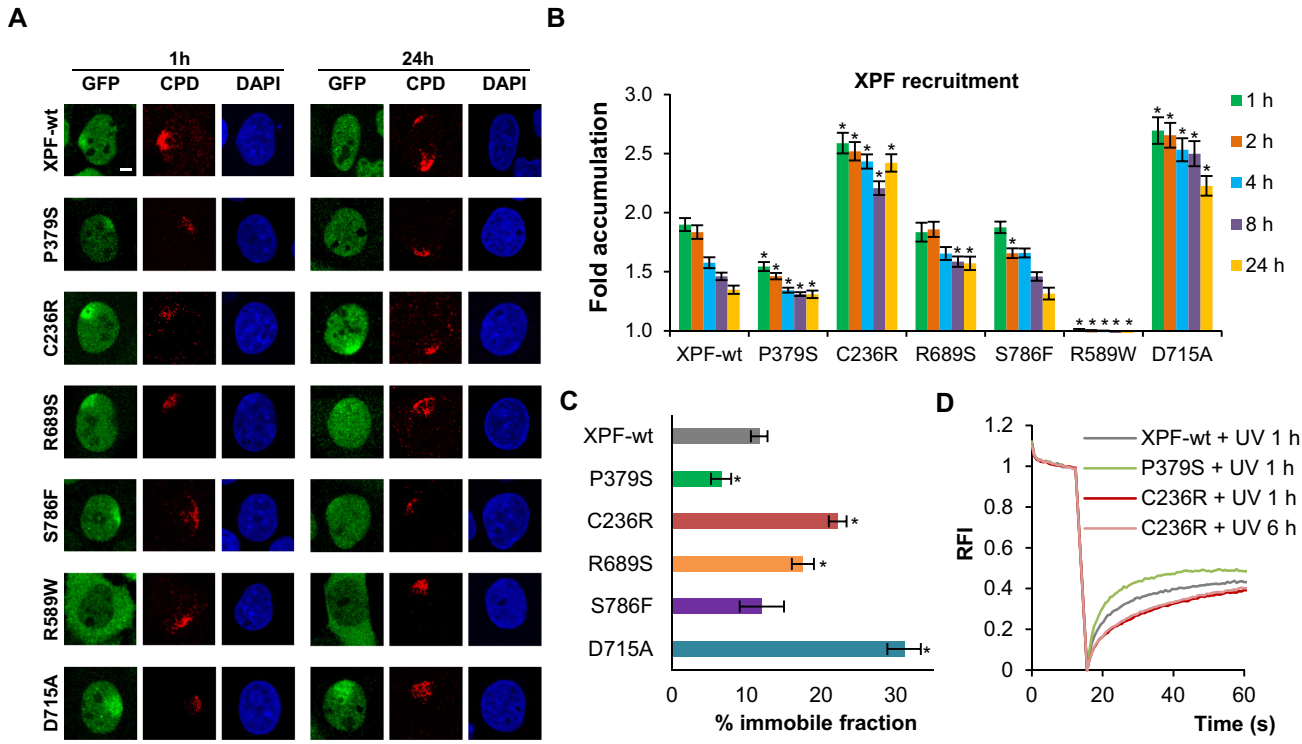

Figure 3. XPF-P379S shows diminished and XPF-C236R persistent DNA damage recruitment. (**A**) Representative immunofluorescence pictures of LUD recruitment of XPF-wt and XPF mutants 1 h and 24 h after local UV irradiation (60 J/m^2) through an 8 μm microporous filter. Cells were stained with antibodies against GFP and CPD, as damage marker. Cells showing clear and comparable local CPD staining are depicted. Scale bar: 5 μm. (**B**) Quantification of LUD recruitment of XPF-wt and XPF mutants, at 1, 2, 4, 8 and 24 h after UV irradiation (60 J/m^2) through a microporous filter, determined by immunofluorescence as shown in (A) and in Supplementary Figure S2A. The fold accumulation was calculated by normalizing fluorescence intensity at sites of local damage to the nuclear background and plotted as average of at least 60 cells per condition from two independent experiments. Statistical significant difference ($P < 0.05$) compared to wt for each time point is indicated by *. (**C**) Percentage immobile fraction of XPF-wt and XPF mutants following UV irradiation (5 J/m^2), as determined by FRAP analysis, shown in Supplementary Figure S2B, of at least 20 cells per condition from at least two independent experiments. Statistical significant difference ($P < 0.05$) compared to wt is indicated by *. In (B) and (C), error bars represent the SEM. (**D**) FRAP analysis of XPF-wt, XPF-P379S (1 h after UV) and XPF-C236R (1 and 6 h after UV) accumulated at LUD, inflicted by 60 J/m^2 UVC through an 8 μm microporous filter. Each curve represents the average of 30 cells per condition from at least three different experiments. RFI indicates relative fluorescence intensity.

a marker for sites of UV damage because CPDs are only very slowly repaired in human cells (43) and still visible up to 24 h after DNA damage induction. XPF-wt clearly accumulated at 1 h and 2 h after UV and showed gradual diminished recruitment at later time points (Figure 3A-B and Supplementary Figure S2A). XPF-R689S and XPF-S786F showed similar recruitment kinetics, albeit XPF-R689S showed slightly delayed release from sites of damage. In contrast, XPF-P379S was inefficiently recruited to LUD at early time points whereas its recruitment also gradually diminished at later time points. Strikingly, XPF-C236R, as well as the nuclease dead XPF-D715A, were strongly recruited at all time points and, remarkably, still persisted at LUD at 24 h. XPF-R589W did not accumulate at all to LUD, even in cells that showed some nuclear localization of the mutant protein, confirming that this is a null mutation.

To further study the dynamic interaction of each of the XPF mutants with UV-irradiated, damaged chromatin, we performed fluorescence recovery after photobleaching (FRAP) in untreated and UV treated cells immediately after irradiation. In untreated cells, all tested XPF mutants showed comparable mobility to XPF-wt, indicating that the mutations do not interfere with XPF's ability to freely move through the nucleus (Supplementary Figure S2B). XPF-R589W could not be tested because its nuclear expression was too low to perform FRAP. Upon UV treatment, incomplete fluorescence recovery of XPF-wt was observed due to XPF immobilization on UV-damaged chromatin, reflecting active participation in NER (33). The fraction of immobilized wild type XPF after 5 J/m^2 UVC was calculated to be around 12% (Figure 3C). Similar UV-induced immobilization was observed for XPF-S786F while XPF-R689S showed increased immobilization compared to wild type, in accord with its slightly delayed release from LUD observed with immunofluorescence (Figure 3C and Supplementary Figure S2B). Also in line with the immunofluorescence, we observed diminished UV-induced immobilization for XPF-P379S, suggesting that this XP mutant is not efficiently recruited or less stably bound to UV damage. In contrast, XPF-C236R and XPF-D715A showed much stronger UV-induced immobilization than XPF-wt. These data, together with the prolonged LUD accumulation observed in immunofluorescence, indicate that although both mutants are efficiently recruited by the NER machinery, their release from UV damage sites is impaired. This prolonged reten-

tion at UV damage sites is likely because both mutants cannot efficiently incise damaged DNA during NER, as it was found that the C236R and D715A mutations respectively reduce (15) and disrupt (8) XPF endonuclease activity *in vitro*.

Because of the strong and prolonged accumulation of XPF-C236R at LUD sites, we investigated if in time this mutant becomes permanently bound to sites of damage or if it is still dynamically binding and dissociating. To this aim, we performed FRAP on LUD inflicted through a microporous filter to measure the mobility (association/dissociation) of XPF-C236R at sites of DNA damage 1 and 6 h after irradiation. As comparison, we measured the mobility of XPF-wt and XPF-P379S on LUD 1 h after UV. Although mutant XPF-P379S was capable of accumulating at LUD (in reduced amounts), its faster recovery of fluorescence after bleaching as compared to XPF-wt (Figure 3D) suggests that this mutant is swiftly exchanged with non-bound XPF. Recruitment and binding of ERCC1-XPF to damaged DNA is thought to be mediated by an interaction of ERCC1 with XPA (9,10,44,45), while XPF activity may be stimulated by an interaction with RPA (46). Thus, it may be that a mutated ERCC1-XPF-P379S complex has reduced affinity for one of these proteins or is less well able to bind to DNA. Interestingly, XPF-C236R at both the 1 and 6 h time points after UV showed increased initial immobilization but its fluorescence slowly recovered in time (the ascending slope of the FRAP curve in Figure 3D), reflecting delayed but still continuous dissociation. These data confirm that XPF-P379S is inefficiently incorporated into the NER incision complex. Conversely, XPF-C236R is not released as efficiently as XPF-wt, i.e. as when damage is excised, but it likely associates and dissociates continuously to deal with persistent NER substrates.

The NER machinery is continuously recruited to DNA damage in the absence of XPF incision

Next, we investigated how the different recruitment behavior of XPF-P379S and XPF-C236R affects the DNA damage recruitment of upstream NER factors, using immunofluorescence. In cells expressing XPF-wt and XPF-P379S, XPC, XPB, XPG and XPA (Figure 4) clearly accumulated at sites of local damage, marked by CPD staining, 1 h after UV and had disappeared after 8 h. In contrast, in XPF KO cells and cells expressing XPF-C236R, as well as in cells expressing catalytically inactive XPF-D715A, accumulation of these NER factors was still clearly visible 8 h after UV. Moreover, also in cells expressing the XPF-R589W null mutant in the nucleus, XPB localization at LUD persisted up to 8 h after UV (Figure 4C). As LUD recruitment of TC-NER factors, such as CSB, is difficult to visualize using immunofluorescence, we measured chromatin binding of CSB after UV using cellular fractionation. CSB was strongly enriched in chromatin of all cells 1 h after irradiation but showed delayed release from chromatin in XPF-P379S and XPF-C236R expressing cells, which was strongest for XPF-C236R (Figure 5). Taken together, these data indicate that in the absence of XPF-mediated incision, also upstream NER factors XPC, TFIIH, XPA, XPG and CSB are continuously recruited to sites of damage and/or less efficiently dissociated, likely in a vain attempt to repair persisting lesions.

XPF-P379S still allows slow repair while XPF-C236R blocks repair

To explore how NER activity itself is affected by XPF-P379S and XPF-C236R, we determined TC- and GG-NER capacity by measuring respectively recovery of RNA synthesis (RRS) after UV-induced transcription inhibition and unscheduled DNA synthesis (UDS) after UV in XPF KO cells expressing both mutant proteins. RRS, quantified by measuring 5-ethynyluridine (EU) incorporation into RNA 24 h after UV, showed that TC-NER was severely affected in XPF KO and XPF-C236R cells but not in cells expressing XPF-wt or XPF-P379S (Figure 6A). UDS was determined by quantifying incorporation of 5-ethynyl-2-deoxiuridine (EdU) for 30 and 60 min. We measured EdU levels at LUD sites, to be sure that UDS measurements were not obscured by EdU incorporated during replication in the rapidly proliferating U2OS cells. UDS levels in XPF-P379S cells increased from 30 to 60 min but were lower than in XPF-wt cells, indicating that repair took place but less efficiently. However, strikingly, XPF-C236R cells only showed baseline UDS levels that did not increase in time, suggesting that these cells are severely deficient in GG-NER (Figure 6B). To confirm this, we measured clearance of CPD lesions in 24 h by immunofluorescence after global UV irradiation of cells. This showed that CPDs are indeed repaired in XPF-P379S cells, although with slight delay as compared to U2OS and XPF-wt cells (Figure 6C). Both XPF KO and XPF-C236R cells did not repair CPDs. These results indicate that the C236R mutation leads to a much stronger NER defect than the P379S mutation, causing impaired transcription after DNA damage, which may very well explain the more severe and CS-like features in patients carrying this mutation.

Continuous recruitment of the NER machinery is a common feature of XPCS cells

To verify that also in XPCS complex patient cells the NER machinery persistently binds to DNA damage, we tested the DNA damage recruitment of XPF and XPB in CS1USAU and XPCS1CD fibroblasts that carry the C236R mutation in XPF (Table 1) (15). XPF and XPB clearly co-localized in nuclear LUD foci in wild type C5RO fibroblasts as well as in the XPCS fibroblasts 1 h after UV (Figure 7A). No co-localization was observed 8 h after UV in wild type fibroblasts, due to removal of lesions, but intriguingly the co-localization did not disappear in XPCS cells.

Next, we investigated whether persistent recruitment of NER proteins is a specific feature also of other XPCS complex patient fibroblasts, which is not observed in cells from patients affected by XP only, and whether similar persistent recruitment can be observed in cells from severe DSC syndrome. Therefore, we tested the LUD recruitment of XPC, TFIIH subunits XPB and XPD, XPA, XPG and XPF in XP patient fibroblasts carrying mutations in XPD or XPF, in XPCS complex patient fibroblasts carrying mutations in *XPB*, *XPD*, *XPG* or *XPF* and in DSC patient fibroblasts carrying a mutation in *XPA*. In wild type and XP fibrob-

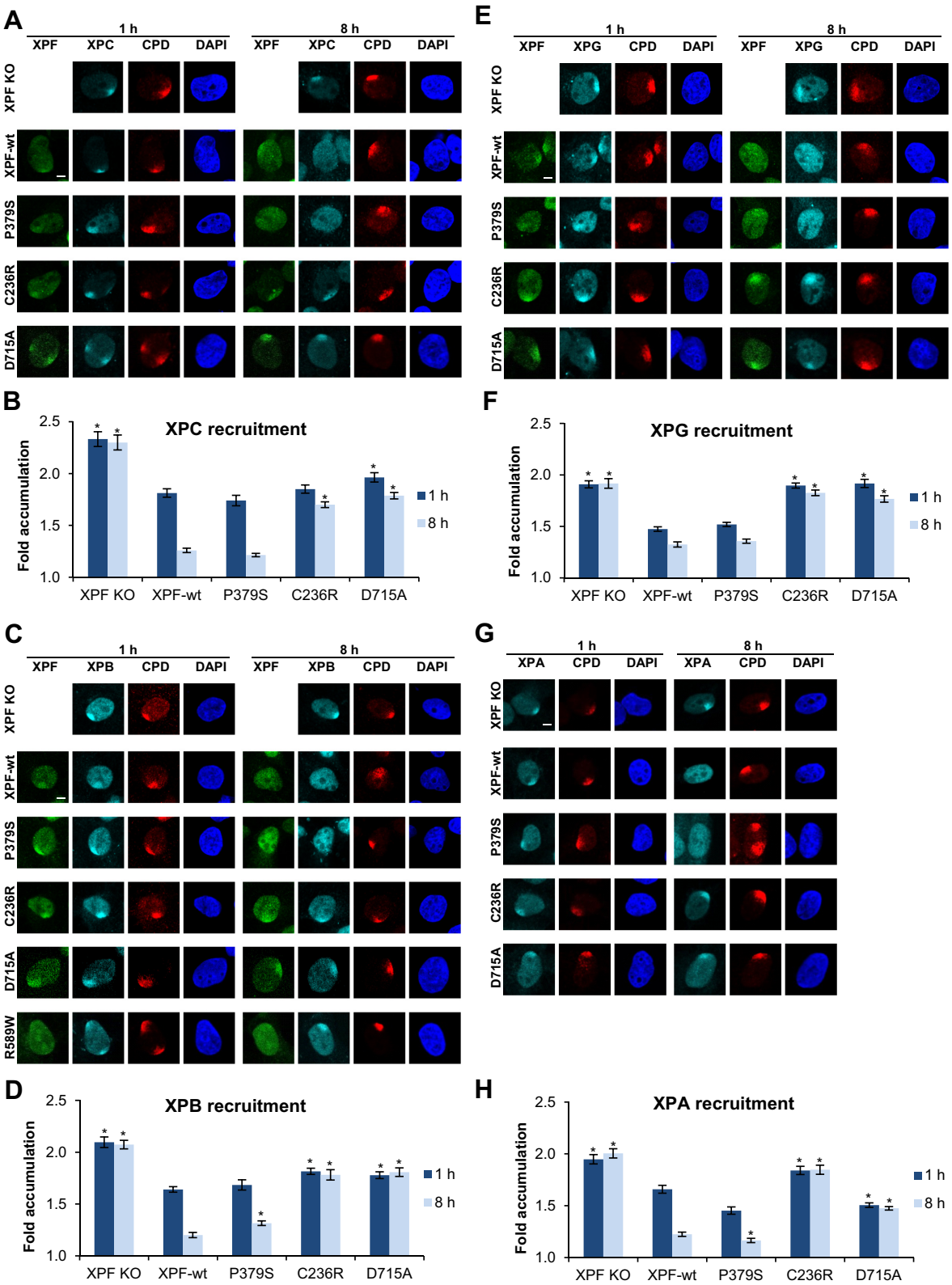

Figure 4. The NER machinery is continuously recruited at sites of DNA damage in XPF KO and XPF-C236R expressing cells. Representative immunofluorescence pictures and quantification of LUD recruitment of XPC (**A** and **B**), XPB (**C** and **D**), XPG (**E** and **F**) and XPA (**G** and **H**) 1 h and 8 h after 60 J/m^2 UVC irradiation through an 8 μm microporous filter in XPF KO cells and cells expressing XPF-wt, XPF-P379S, XPF-C236R, XPF-D715A and (only in C) XPF-R589W. UV damage was visualized by CPD staining. Scale bar: 5 μm. Fold accumulation was calculated by normalizing fluorescence at sites of local damage to the nuclear background and plotted as average of at least 111 (XPC), 85 (XPB), 137 (XPG) and 105 (XPA) cells per condition from at least two independent experiments. Statistical significant difference ($P < 0.05$) compared to wt for each time point is indicated by *.

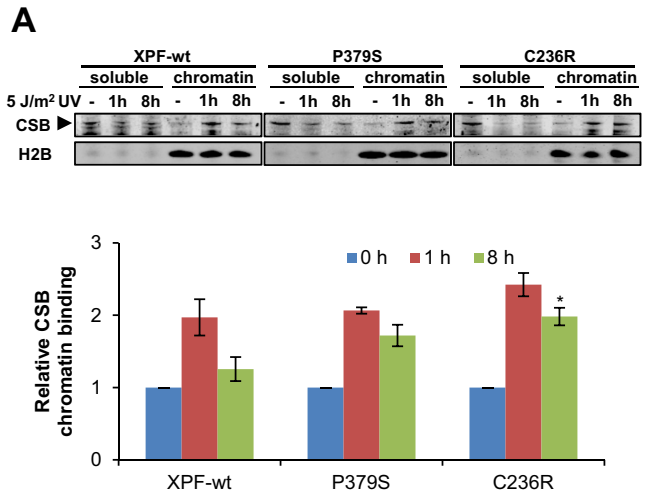

Figure 5. Delayed CSB release from chromatin in XPF-P379S and XPF-C236R cells. Representative cell fractionation of XPF-wt, XPF-P379S and XPF-C236R cells analyzed by immunoblot against CSB and H2B (as loading control; upper panel). Cells were mock treated (–) or irradiated with 5 J/m^2 UVC, lysed after 1 h and 8 h and fractionated into non-chromatin bound (soluble) and chromatin-bound proteins. Lower panel shows quantified levels of CSB bound to the chromatin relative to H2B averaged from four independent experiments. Error bars indicate SEM. Statistical significant difference ($P < 0.05$) compared to wt for each time point is indicated by *.

lasts, XPC, XPB, XPD, and XPG localized to sites of damage 1 h after UV and had (mostly) disappeared at 8 h (Figure 7B and Supplementary Figures S3 and S4; Table 2). Similar transient recruitment was observed for XPA in wild type and XPF-deficient XP cells, but XPA recruitment was not observed in XPD-deficient XP cells (Supplementary Figure S5), likely because XPA acts downstream of TFIIH. XPF LUD recruitment was not clearly visible in the XPF-deficient XP-patient cells XP32BR, expressing R589W and P379S mutant XPF, and XP42RO, expressing XPF with a R799W mutation. This result is in line with the diminished recruitment we had observed for XPF-P379S and may indicate that, similarly, XPF carrying a R799W mutation is less efficiently recruited. In contrast, in XPCS cells, we observed persistent DNA damage recruitment of XPC, XPB and XPD at 8 h after UV. Persistent XPA and XPF recruitment was only clearly observed in XPF- and XPG-deficient XPCS cells, but not in XPB- and XPD-deficient cells. XPG also persisted at LUD in XPF-deficient XPCS cells but its recruitment, even at 1 h, could hardly be discerned in XPB- and XPD-deficient XPCS cells. Intriguingly, DSC patient fibroblasts also showed persistent recruitment of XPC, XPB and XPD. These data indicate that continuous DNA damage recruitment of part of the core NER machinery, i.e. XPC and TFIIH, is a general feature of cells derived from XP patients showing additional CS features and/or severe growth and progressive neurological defects.

DISCUSSION

As most ERCC1-XPF patient mutations manifest as compound heterozygous, obscuring a clear understanding of their individual pathogenic impact, we individually expressed XPF mutants in XPF KO cells to study how each mutation affects ERCC1-XPF activity in NER. XP-associated P379S mutant XPF, which in patients is found homozygous or heterozygous with a silent allele or the null allele R589W (Table 1) (19,39), was inefficiently recruited to DNA damage. Still, this mutant conserved significant residual repair capacity, as shown by increasing UDS levels and repair of CPDs in time. Thus, P379S does not fully abolish but only slows down NER, explaining the almost complete transcription recovery after UV and very mild UV sensitivity observed with this mutant. This is in agreement with significant UDS levels reported for XP72BR, XP7NE and XP32BR patient fibroblasts carrying this mutation (19,39) (Table 1). Intriguingly, Fassihi *et al.* noticed that P379S occurs with a high allele frequency of 0.3% in the SNP database which would predict more homozygous P379S individuals than patients currently diagnosed with XP (39). Our results, showing that this mutation only mildly impairs ERCC1-XPF activity in NER, might explain this disparity. Residual GG-NER activity has also been reported in cells expressing another XP-associated XPF mutant, i.e. R799W (16,19,24). In XP42RO fibroblasts expressing this mutant, we hardly observed DNA damage XPF recruitment but also did not notice persistent recruitment of the upstream NER

Table 2. Localization of NER factors to LUD in XP, XPCS and DSC patient fibroblasts.

disease	cell line	gene affected	1 h XPC	8 h XPC	1 h XPB	8 h XPB	1 h XPD	8 h XPD	1 h XPA	8 h XPA	1 h XPG	8 h XPG	1 h XPF	8 h XPF
	C5RO		+	-	+	-	+	-	+	-	+-	-	+	-
XP	XP42RO	XPF (R799W)	+	-	+	-	+	+-	+	-	+	-	-	-
XP	XP32BR	XPF (R589W P379S)	+	-	+	-	+	-	+	-	+	-	-	-
XP	XP6BE	XPD (R683W)	+	-	+-	+-	+	-	-	-	+-	+-	+-	-
XPCS	XPCS1CD	XPF (C236R R589W)	+	+	+	+	+	+	+	+	+	+	+	+
XPCS	XPCS1BA	XPB (F99S)	+	+	+-	+-	+	+	-	-	-	-	+-	-
XPCS	XPCS2	XPD (G602D)	+	+-	+	+-	+	+	+	+-	+-	+-	+	-
XPCS	XPCS1RO	XPG (926fs)	+	+	+	+	+	+	+	+	-	-	+	+
DSC	XP25RO	XPA (R207X)	+	+	+	+	+	+	-	-	+	-	-	-

+(almost) always visible.
+-intermediate visible.
-not or hardly visible.
XP: xeroderma pigmentosum.
XPCS: xeroderma pigmentosum-Cockayne syndrome.
DSC: De Sanctis Cacchione.

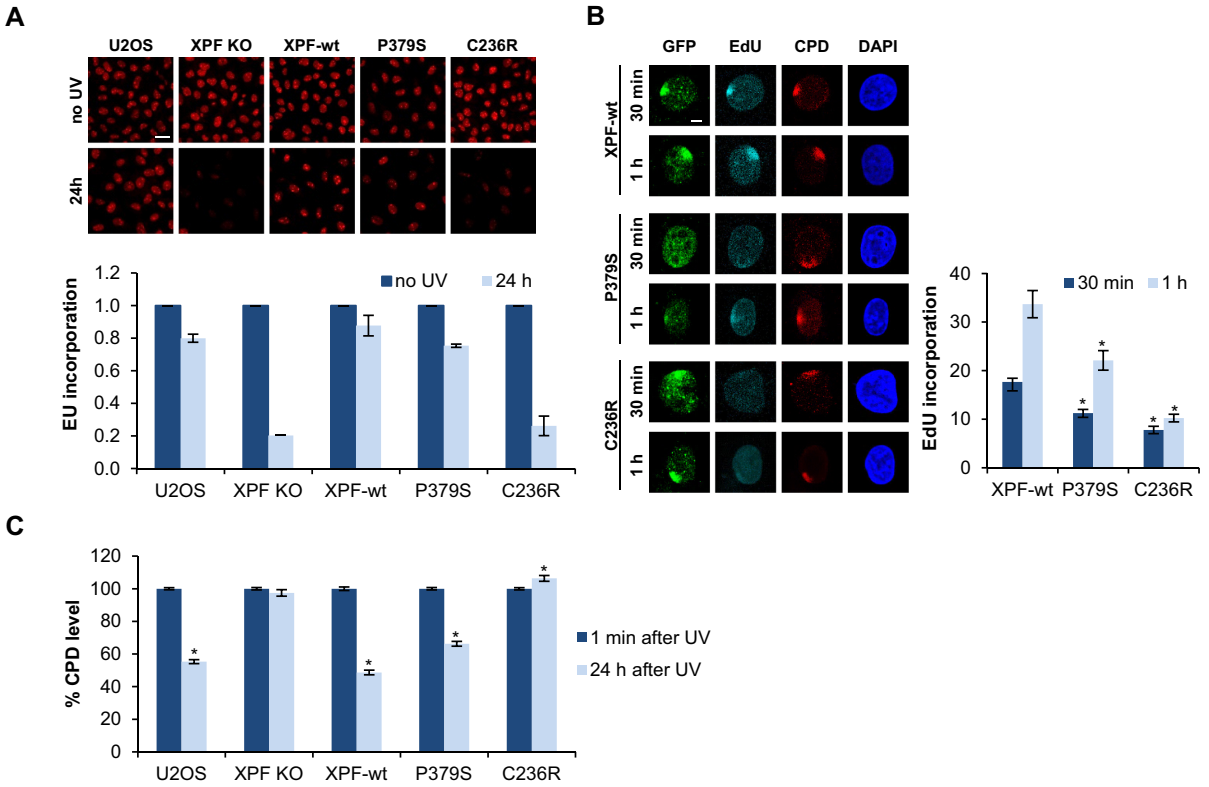

Figure 6. NER is delayed by XPF-P379S and strongly inhibited by XPF-C236R. (**A**) RRS measured by EU incorporation 24 h after mock-treatment (no UV) or 6 J/m^2 UVC in U2OS, XPF KO and XPF-wt, XPF-P379S and XPF-C236R expressing cells. Upper panel shows representative images of red nuclear EU staining. Lower panel shows quantified EU incorporation levels averaged from at least 100 cells in two independent experiments. Scale bar: 25 μm. (**B**) UDS determined by measuring EdU incorporation at LUD sites for 30 min and for 1 h after UV irradiation (60 J/m2) inflicted through an 8 μm microporous filter. Left panel shows representative images of cells stained for EdU (cyan) and CPD (red). Right panel shows quantified EdU incorporation levels averaged from at least 60 cells from two independent experiments. Scale bar: 5 μm. (**C**) CPD removal, as determined by immunofluorescence in U2OS, XPF KO cells and cells expressing XPF-wt, XPF-P379S and XPF-C236R 1 min and 24 h after irradiation with 10 J/m^2 UVC. CPD levels were measured from at least 277 cells from two independent experiments, averaged and normalized to levels 1 min after UV irradiation. Statistical significant difference ($P < 0.05$) compared to wt for each time point (B) or compared to 1 min after UV (C) is indicated by *.

machinery (Figure 7B and Supplementary Figures S3–S5) as in XPF KO and nuclease-dead XPF-D715A cells, suggesting that NER is not completely impaired. Similarly, residual but slower NER activity was reported for mild XP patient cells from XP complementation groups other than *XP-F* (47–52). Our data therefore support the idea that mild XP symptoms result from mutations in NER genes that reduce, but do not abolish, GG-NER activity (Figure 8).

XPF mutation C236R was identified in two XPCS patients, either as compound heterozygous with R589W or with an allele encoding a barely expressed truncated XPF lacking its nuclease domain (Table 1) (15). Strikingly, this mutation affected XPF activity in NER much more severely than P379S. Similarly to nuclease-dead XPF-D715A, XPF-C236R was persistently recruited to DNA damage (up to 24 h). This was confirmed by FRAP analyses, which, however, indicated that XPF-C236R is not statically bound to damaged DNA. If a fraction of XPF-C236R was statically bound, its fluorescence recovery in LUD (as measured in Figure 3D) would be expected to reach a steady-state plateau below the level of XPF-wt, whereas instead we observed continued recovery (i.e. an ascending slope), albeit delayed, of the fluorescence signal in time. Thus, considering also the reduced nuclease activity *in vitro* and the low UDS, RRS and CPD repair levels associated with this mutation, as observed in our cells and previously in patient fibroblasts (15) (Table 1), we speculate that C236R mutant XPF likely continuously binds and dissociates from sites of damage because it is incapable of efficiently incising DNA. In XPF-C236R as well as in XPF-D715A and XPF KO cells, in which obviously no incision is made, the core NER factors XPC, CSB, TFIIH, XPA and XPG were also persistently recruited to sites of damage. It is therefore likely that in XPF-C236R cells the repair reaction is severely blocked (Figure 8). The continuous presence of the core NER machinery probably reflects a futile attempt to build up a functional NER complex, which is also continuously aborted because of the absence of functional XPF. Strikingly, we observed the same persistent recruitment of part of the core NER machinery in XPCS patient fibroblasts from different XP complementation groups as well as in DSC XPA-deficient cells, likely because in these cells NER is strongly blocked as well. Thus, a major difference between mutations that cause only mild XP and mutations that cause additional developmental and progressive neurodegenerative symptoms might be that these latter mutations much more strongly reduce, or even abolish, NER. Such strongly or completely impaired NER may elicit more untoward events

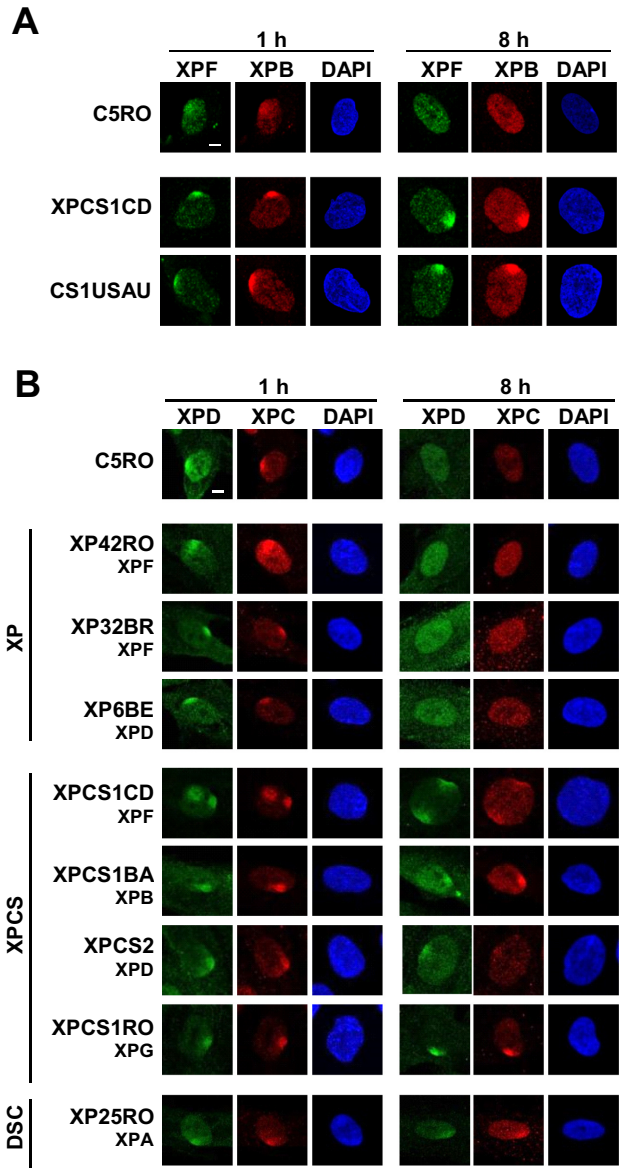

Figure 7. XPC and TFIIH are continuously recruited to UV damage in XPCS patient fibroblasts. (**A**) Representative immunofluorescence pictures showing the co-localization of XPF and XPB at LUD in patient fibroblasts XPCS1CD and CS1USAU, compared to wild type C5RO fibroblasts. Cells were stained 1 h and 8 h after local UV irradiation (60 J/m^2) through an 8 μm microporous filter with antibodies against XPF and XPB. (**B**) Representative immunofluorescence pictures showing the LUD recruitment of XPD and XPC in fibroblasts derived from patients carrying mutations in XPB, XPD, XPG, XPF and XPA, affected by mild XP (XP42RO, XP32BR, XP6BE), XPCS (XPCS1CD, XPCS1BA, XPCS2, XPCS1RO) or DSC (XP25RO) compared to wild type C5RO fibroblasts. Cells were locally UV irradiated with 60 J/m^2 UVC through an 8 μm microporous filter and stained 1 h and 8 h after irradiation with antibodies against XPD and XPC. Scale bar: 5 μm.

than simply failure to prevent mutagenesis, thus contributing to the more severe phenotype observed in XPCS and DSC.

In the absence of NER, recovery of lesion-stalled transcription is impeded. This could possibly be exacerbated because the NER machinery is continuously binding the same lesion in a vain attempt of repair. As a side consequence, lesions may become less accessible to other repair mechanisms, leading to permanent transcription and possibly also replication defects. This is in line with a model previously proposed for CS in which RNA polymerase II stuck on lesions renders lesions inaccessible to any repair mechanism (6). Unrepaired lesions interfering with transcription and replication will cause a persistent DNA damage response and may induce specific cell fate decisions, leading to senescence or cell death, which might contribute to the more severe phenotypes observed in XPCS while reducing cancer incidence as compared to XP (3,6). Also, continuous recruitment and activation of the NER machinery may hyperactivate PARP, causing continuous PAR recycling and thus higher ATP consumption, which might ultimately contribute to defective mitophagy often connected to neurodegeneration observed in CS or DSC (53). Additionally, prolonged binding of DNA damage by TFIIH was previously proposed to lead to extensive ssDNA formation contributing to DNA break formation and genomic instability, as observed in mouse and human XPD-XPCS cells (54,55). Based on structural analysis of a distantly related XPD ortholog from *Sulfolobus acidocaldarius* (56), it was hypothesized that XPD-XPCS mutations may reduce the flexibility of XPD and force the protein in an abnormal conformation that compromises TFIIH function in TC-NER, leading to CS features (57). XP mutations in XPD, on the other hand, may only reduce helicase activity and DNA binding, making NER less efficient, leading to XP and cancer. Mutational analysis in *S. cerevisiae* furthermore suggested that XPD-XPCS mutations still allow partial DNA unwinding by TFIIH, increasing its affinity towards DNA and leading to its permanent recruitment at sites of damage, leaving TFIIH unavailable for transcription resumption (58). Our results also resemble those observed in mouse models with different XPG mutations. Mice carrying a point mutation in XPG that is predicted to affect its endonuclease activity (D811A) show severe, but not completely impaired 6-4PP lesion removal and UV survival and no CS features (59). In contrast, mice which XPCS mimicking truncating XPG mutations or lacking XPG show stronger defects in lesion removal and UV survival and display a CS phenotype. Such severe truncating mutations in XPG have, however, also been noted to affect other processes besides NER, which may be causative for (part of) the CS phenotype. For instance, severe C-terminal truncation of XPG was suggested to affect its stabilization of TFIIH, leading to dysregulation of gene expression (60), and its non-enzymatic role in regulating homologous recombination and BRCA1 function (61). Similarly, it could be that severe mutations in XPF affect other processes besides NER. For instance, besides its role in DNA repair, ERCC1-XPF has been implicated in control of gene expression by chromatin looping (together with XPG) (62) and transcription initiation during postnatal development (63), in which the DNA substrate on which ERCC1-XPF acts may be similar as in NER. Thus, the inability of XPF-C236R to incise DNA or its persistence at DNA damage sites may impair these processes as well and lead to (some of the) CS features. All of the different, not mutually exclusive, models proposed to explain the severe XPCS phe-

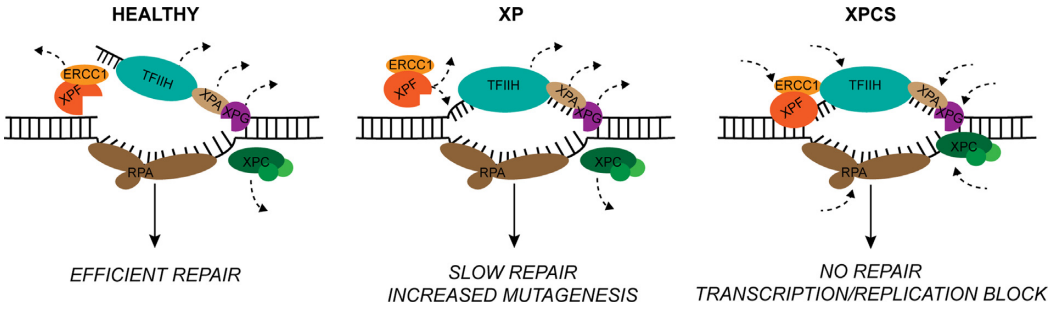

Figure 8. Model showing the difference in NER between XPF-deficient XP and XPCS cells. Left: Wild-type XPF allows efficient recruitment, endonucleolytic function and subsequent release (symbolized by the dashed arrows) of ERCC1-XPF and other NER factors, resulting in efficient repair. Middle: In XP cells with mutated XPF, such as in cells expressing the P379S mutant, XPF is less efficiently recruited to DNA damage. Repair still takes place but at a lower rate and the NER machinery is able to dissociate normally from sites of DNA damage. As a consequence, lesions are less efficiently removed, leading to increased mutagenesis and symptoms associated with XP. Right: In contrast, in XPCS cells with mutated XPF, such as in cells expressing the C236R mutant, the repair reaction is severely blocked. As a consequence, the core NER machinery persistently binds to lesions, likely in a futile attempt to build up a functional NER complex. Impaired repair and persistence of the NER machinery at DNA lesions may enhance transcription impairment due to stalled RNA polymerase II and lead to replication defects, triggering senescence and apoptosis rather than cancer, causing the additional and severe symptoms found in XPCS patients. The same persistent recruitment of part of the core NER machinery is observed in XPCS patient fibroblasts from different XP complementation groups as well as in DSC XPA-deficient cells.

notype suggest severe disturbance of the normal activity of multifunctional NER factors that eventually compromises chromatin-associated processes. Our data further expand these models by showing that persistent assembly of advanced but non-functional NER pre-incision complexes may strongly interfere with chromatin-associated processes, including transcription which is severely impaired after UV-damage in XPF-C236R and XPF KO cells.

The advantage of our XPF KO system for studying functionality of single XPF mutants is clearly illustrated by analysis of the R589W mutation, which is found in both mild and severe XP and XPCS patients as heterozygous combination with P379S, R799W, C236R or an exon 3 deletion (Table 1) (15,19,39). XPF with this mutation localized predominantly in the cytoplasm and was unable to bind DNA damage or rescue UV and MMC sensitivity of XPF KO cells, clearly indicating that R589W can be considered as a functional null mutation. Its cytoplasmic localization is in line with the previously observed cytoplasmic XPF localization in patient fibroblasts expressing this mutant (19). It is thus likely that differences in symptoms observed in patients carrying this mutation are mainly derived from differences in the capacity of the other affected XPF allele to function in NER. Thus, patients carrying P379S besides R589W (e.g. XP32BR; Table 1) will have residual repair and exhibit mild XP symptoms, whereas patients carrying C236R besides R589W (e.g. XPCS1CD; Table 1) will hardly have repair and therefore exhibit additional CS symptoms.

Finally, we analyzed two nuclease domain mutations not implicated in XP or XPCS but associated with defects in ICLR and FA. S786F, identified in a breast cancer, was shown to sensitize cells to MMC, but not to UV (40), and to lead to defective ICL unhooking in *Xenopus laevis* egg extracts (20), which was confirmed by our damage recruitment and UV and MMC survival analyses. R689S was found in an FA patient together with an allele encoding a non-expressed frameshift XPF mutant. Both the absence of typical XP features as well as analysis of patient fibroblasts suggested that R689S renders XPF fully defective in ICLR but only partially defective in NER (16) (Table 1). This was confirmed by mild UV but strong MMC hypersensitivity we observed for XPF-R689S expressing cells. Previously, mutation of R689 in human and its equivalent residue in *Xenopus laevis* XPF was shown to reduce XPF nuclease activity *in vitro* and to diminish UV lesion removal (8,20,64). In accordance, we noticed slightly increased UV-induced immobilization and delayed damage dissociation of XPF-R689S. These results might therefore indicate that NER is mildly retarded by this mutation because XPF is slightly less able to perform DNA incision, possibly because of defects in positioning of active site residues that carry out this incision (64).

In summary, our analysis indicates that impaired repair and persistence of the NER machinery at DNA lesions characterizes cells from XP patients exhibiting additional developmental and neurodegenerative symptoms (Figure 8). Possibly, the continuous targeting of the core NER machinery to lesions further enhances transcription impairment due to stalled RNA polymerase II, resulting in additional CS-like features. It has always been difficult to grasp how mutations within the same repair pathway and even within the same gene lead to the complex and pleiotropic features associated with hereditary defects in NER, especially since many mutations occur in varying compound heterozygous combinations. Our functional analysis of single XPF mutants exemplifies the advantage of separately studying the impact of each individual allele. The current advance of precise genome editing techniques will likely ease and speed up similar approaches to scrutinize mutations in other NER genes, leading to improved understanding of the molecular mechanisms that underlie different DNA repair disorders.

SUPPLEMENTARY DATA

Supplementary Data are available at NAR Online.

ACKNOWLEDGEMENTS

The authors would like to thank Dr Gijsbert J. van Belle for advice, Ciske Bertens for technical assistance, Dr Or-

lando D. Schärer for providing XPF cDNA, Dr Tomoo Ogi for cell lines XPCS1CD and CS1USAU. We are also thankful to the Erasmus MC Optical Imaging Center for support with microscopes.

FUNDING

Marie Curie Initial Training Network 'aDDRess' funded by the European Commission 7th Framework Programme [316390]; European Research Council Advanced Grant [340988-ERC-ID to W.V.]; EMBO long-term fellowship [ALTF 663-2014 to J.S]; Dutch Cancer Society [10506]; Oncode Institute which is partly financed by the Dutch Cancer Society and was funded by the gravitation program CancerGenomiCs.nl from the Netherlands Organization for Scientific Research (NWO). Funding for open access charge: European Research Council.
Conflict of interest statement. None declared.

REFERENCES

1. Lehmann,A.R., McGibbon,D and Stefanini,M. (2011) Xeroderma pigmentosum. *Orphanet J. Rare Dis.*, **6**, 1–6.
2. Natale,V. (2011) A comprehensive description of the severity groups in Cockayne syndrome. *Am. J. Med. Genet. A*, **155**, 1081–1095.
3. Natale,V. and Raquer,H. (2017) Xeroderma pigmentosum-Cockayne syndrome complex. *Orphanet. J. Rare Dis.*, **12**, 65.
4. Kraemer,K.H., Patronas,N.J., Schiffmann,R., Brooks,B.P., Tamura,D. and DiGiovanna,J.J. (2007) Xeroderma pigmentosum, trichothiodystrophy and Cockayne syndrome: A complex genotype-phenotype relationship. *Neuroscience*, **145**, 1388–1396.
5. Rahbar,Z. and Naraghi,M. (2015) De Sanctis–Cacchione syndrome: A case report and literature review. *Int. J. Women's Dermatol.*, **1**, 136–139.
6. Marteijn,J.A., Lans,H., Vermeulen,W. and Hoeijmakers,J.H.J. (2014) Understanding nucleotide excision repair and its roles in cancer and ageing. *Nat. Rev. Mol. Cell Biol.*, **15**, 465–481.
7. Schärer,O.D. (2013) Nucleotide excision repair in Eukaryotes. *Cold Spring Harb. Perspect. Biol.*, **5**, a012609.
8. Enzlin,J.H. and Schärer,O.D. (2002) The active site of the DNA repair endonuclease XPF-ERCC1 forms a highly conserved nuclease motif. *EMBO J.*, **21**, 2045–2053.
9. Manandhar,M., Boulware,K.S. and Wood,R.D. (2015) The ERCC1 and ERCC4 (XPF) genes and gene products. *Gene*, **569**, 153–161.
10. Tsodikov,O. V, Ivanov,D., Orelli,B., Staresincic,L., Shoshani,I., Oberman,R., Schärer,O.D., Wagner,G. and Ellenberger,T. (2007) Structural basis for the recruitment of ERCC1-XPF to nucleotide excision repair complexes by XPA. *EMBO J.*, **26**, 4768–4776.
11. Sijbers,A.M., De Laat,W.L., Ariza,R.R., Biggerstaff,M., Wei,Y.F., Moggs,J.G., Carter,K.C., Shell,B.K., Evans,E., De Jong,M.C. *et al.* (1996) Xeroderma pigmentosum group F caused by a defect in a structure-specific DNA repair endonuclease. *Cell*, **86**, 811–822.
12. Bhagwat,N., Olsen,A.L., Wang,A.T., Hanada,K., Stuckert,P., Kanaar,R., D'andrea,A., Niedernhofer,L.J. and Mchugh,P.J. (2009) XPF-ERCC1 participates in the fanconi anemia pathway of Cross-Link repair. *Mol. Cell. Biol.*, **29**, 6427–6437.
13. Klein Douwel,D., Boonen,R.A.C.M., Long,D.T., Szypowska,A.A., Räschle,M., Walter,J.C. and Knipscheer,P. (2014) XPF-ERCC1 acts in unhooking DNA interstrand crosslinks in cooperation with FANCD2 and FANCP/SLX4. *Mol. Cell*, **54**, 460–471.
14. Kee,Y. and D'Andrea,A. (2012) Molecular pathogenesis and clinical management of Fanconi anemia. *J. Clin. Invest.*, **122**, 3799–3806.
15. Kashiyama,K., Nakazawa,Y., Pilz,D.T., Guo,C., Shimada,M., Sasaki,K., Fawcett,H., Wing,J.F., Lewin,S.O., Carr,L. *et al.* (2013) Malfunction of nuclease ERCC1-XPF results in diverse clinical manifestations and causes Cockayne syndrome, xeroderma pigmentosum, and Fanconi anemia. *Am. J. Hum. Genet.*, **92**, 807–819.
16. Bogliolo,M., Schuster,B., Stoepker,C., Derkunt,B., Su,Y., Raams,A., Trujillo,J.P., Minguillón,J., Ramírez,M.J., Pujol,R. *et al.* (2013) Mutations in ERCC4, encoding the DNA-repair endonuclease XPF, cause Fanconi anemia. *Am. J. Hum. Genet.*, **92**, 800–806.
17. Niedernhofer,L.J., Garinis,G.A., Raams,A., Lalai,A.S., Robinson,A.R., Appeldoorn,E., Odijk,H., Oostendorp,R., Ahmad,A., Van Leeuwen,W. *et al.* (2006) A new progeroid syndrome reveals that genotoxic stress suppresses the somatotroph axis. *Nature*, **444**, 1038–1043.
18. Jaspers,N.G.J., Raams,A., Silengo,M.C., Wijgers,N., Niedernhofer,L.J., Robinson,A.R., Giglia-Mari,G., Hoogstraten,D., Kleijer,W.J., Hoeijmakers,J.H.J. *et al.* (2007) First reported patient with human ERCC1 deficiency has Cerebro-Oculo-Facio-Skeletal syndrome with a mild defect in nucleotide excision repair and severe developmental failure. *Am. J. Hum. Genet.*, **80**, 457–466.
19. Ahmad,A., Enzlin,J.H., Bhagwat,N.R., Wijgers,N., Raams,A., Appledoorn,E., Theil,A.F., Hoeijmakers,J.H.J., Vermeulen,W., Jaspers,N.G.J. *et al.* (2010) Mislocalization of XPF-ERCC1 nuclease contributes to reduced DNA repair in XP-F patients. *PLoS Genet.*, **6**, e1000871.
20. Klein Douwel,D., Hoogenboom,W.S., Boonen,R.A. and Knipscheer,P. (2017) Recruitment and positioning determine the specific role of the XPF-ERCC1 endonuclease in interstrand crosslink repair. *EMBO J.*, **36**, 2034–2046.
21. Vélez-Cruz,R. and Egly,J.M. (2013) Cockayne syndrome group B (CSB) protein: At the crossroads of transcriptional networks. *Mech. Ageing Dev.*, **134**, 234–242.
22. Karikkineth,A.C., Scheibye-Knudsen,M., Fivenson,E., Croteau,D.L. and Bohr,V.A. (2017) Cockayne syndrome: Clinical features, model systems and pathways. *Ageing Res. Rev.*, **33**, 3–17.
23. Wang,Y., Chakravarty,P., Ranes,M., Kelly,G., Brooks,P.J., Neilan,E., Stewart,A., Schiavo,G. and Svejstrup,J.Q. (2014) Dysregulation of gene expression as a cause of Cockayne syndrome neurological disease. *Proc. Natl. Acad. Sci. U.S.A.*, **111**, 14454–14459.
24. Sijbers,A.M., Van Voorst Vader,P.C., Snoek,J.W., Raams,A., Jaspers,N.G.J. and Kleijer,W.J. (1998) Homozygous R788W point mutation in the XPF gene of a patient with xeroderma pigmentosum and late-onset neurologic disease. *J. Invest. Dermatol.*, **110**, 832–836.
25. Robbins,J.H., Kraemer,K.H., Lutzner,M.A., Festoff,B.W. and Coon,H.G. (1974) Xeroderma pigmentosum: an inherited disease with sun sensitivity, multiple cutaneous neoplasms, and abnormal DNA repair. *Ann. Intern. Med.*, **80**, 221–248.
26. Ellison,A.R., Nouspikel,T., Jaspers,N.G., Clarkson,S.G. and Gruenert,D.C. (1998) Complementation of transformed fibroblasts from patients with combined xeroderma pigmentosum-Cockayne syndrome. *Exp. Cell Res.*, **243**, 22–28.
27. Vermeulen,W., Stefanini,M., Giliani,S., Hoeijmakers,J.H.J. and Bootsma,D. (1991) Xeroderma pigmentosum complementation group H falls into cornplementation group D. *Mutat. Res. DNA Repair*, **255**, 201–208.
28. Scott,R.J., Itin,P., Kleijer,W.J., Kolb,K., Arlett,C. and Muller,H. (1993) Xeroderma pigmentosum-Cockayne syndrome complex in two patients: Absence of slun tumors despite severe deficiency of DNA excision repair. *J. Am. Acad. Dermatol.*, **29**, 883–889.
29. Der Kaloustian,V.M., de Weerd-Kastelein,E.A., Kleijer,W.J., Keijzer,W. and Bootsma,D. (1974) The genetic defect in the De Sanctis-Cacchione syndrome. *J. Invest. Dermatol.*, **63**, 392–396.
30. Sanjana,N.E., Shalem,O. and Zhang,F. (2014) Improved vectors and genome-wide libraries for CRISPR screening. *Nat. Methods*, **11**, 783–784.
31. Brinkman,E.K., Chen,T., Amendola,M. and Van Steensel,B. (2014) Easy quantitative assessment of genome editing by sequence trace decomposition. *Nucleic Acids Res.*, **42**, e168.
32. Campeau,E., Ruhl,V.E., Rodier,F., Smith,C.L., Rahmberg,B.L., Fuss,J.O., Campisi,J., Yaswen,P., Cooper,P.K. and Kaufman,P.D. (2009) A versatile viral system for expression and depletion of proteins in mammalian cells. *PLoS One*, **4**, e6529.
33. Houtsmuller,A.B. (1999) Action of DNA Repair Endonuclease ERCC1/XPF in Living Cells. *Science*, **284**, 958–961.
34. Van Cuijk,L., Van Belle,G.J., Turkyilmaz,Y., Poulsen,S.L., Janssens,R.C., Theil,A.F., Sabatella,M., Lans,H., Mailand,N., Houtsmuller,A.B. *et al.* (2015) SUMO and ubiquitin-dependent XPC exchange drives nucleotide excision repair. *Nat. Commun.*, **6**, 7499.
35. Aydin,Ö.Z., Marteijn,J.A., Ribeiro-Silva,C., Rodríguez López,A., Wijgers,N., Smeenk,G., van Attikum,H., Poot,R.A., Vermeulen,W. and Lans,H. (2014) Human ISWI complexes are targeted by

SMARCA5 ATPase and SLIDE domains to help resolve lesion-stalled transcription. *Nucleic Acids Res.*, **42**, 8473–8485.
36. van Vuuren,A.J., Appeldoorn,E., Odijk,H., Yasui,A., Jaspers,N.G., Bootsma,D. and Hoeijmakers,J.H. (1993) Evidence for a repair enzyme complex involving ERCC1 and complementing activities of ERCC4, ERCC11 and xeroderma pigmentosum group F. *EMBO J.*, **12**, 3693–3701.
37. Biggerstaff,M., Szymkowski,D.E. and Wood,R.D. (1993) Co-correction of the ERCC1, ERCC4 and xeroderma pigmentosum group F DNA repair defects in vitro. *EMBO J.*, **12**, 3685–3692.
38. Volker,M., Moné,M.J., Karmakar,P., Van Hoffen,A., Schul,W., Vermeulen,W., Hoeijmakers,J.H.J., Van Driel,R., Van Zeeland,A.A. and Mullenders,L.H.F. (2001) Sequential assembly of the nucleotide excision repair factors in vivo. *Mol. Cell*, **8**, 213–224.
39. Fassihi,H., Sethi,M., Fawcett,H., Wing,J., Chandler,N., Mohammed,S., Craythorne,E., Morley,A.M.S., Lim,R., Turner,S. *et al.* (2016) Deep phenotyping of 89 xeroderma pigmentosum patients reveals unexpected heterogeneity dependent on the precise molecular defect. *Proc. Natl. Acad. Sci. U.S.A.*, **113**, E1236–E1245.
40. Osorio,A., Bogliolo,M., Fernández,V., Barroso,A., de la Hoya,M., Caldés,T., Lasa,A., Ramón y Cajal,T., Santamariña,M., Vega,A. *et al.* (2013) Evaluation of rare variants in the new fanconi anemia gene ERCC4 (FANCQ) as familial Breast/Ovarian cancer susceptibility alleles. *Hum. Mutat.*, **34**, 1615–1618.
41. Lehmann,J., Seebode,C., Smolorz,S., Schubert,S. and Emmert,S. (2017) XPF knockout via CRISPR/Cas9 reveals that ERCC1 is retained in the cytoplasm without its heterodimer partner XPF. *Cell. Mol. Life Sci.*, **74**, 1–14.
42. Zheng,H., Wang,X., Warren,A.J., Legerski,R.J., Nairn,R.S., Hamilton,J.W. and Li,L. (2003) Nucleotide excision Repair- and Polymerase -Mediated Error-Prone removal of mitomycin C interstrand Cross-Links. *Mol. Cell. Biol.*, **23**, 754–761.
43. Mitchell,D.L., Haipek,C.A. and Clarkson,J.M. (1985) (6–4)Photoproducts are removed from the DNA of UV-irradiated mammalian cells more efficiently than cyclobutane pyrimidine dimers. *Mutat. Res. - Mutat. Res. Lett.*, **143**, 109–112.
44. Li,L., Elledge,S.J., Peterson,C.A., Bales,E.S. and Legerski,R.J. (1994) Specific association between the human DNA repair proteins XPA and ERCC1. *Proc. Natl. Acad. Sci. U.S.A.*, **91**, 5012–5016.
45. Park,C.H. and Sancar,A. (1994) Formation of a ternary complex by human XPA, ERCC1, and ERCC4(XPF) excision repair proteins. *Proc. Natl. Acad. Sci. U.S.A.*, **91**, 5017–5021.
46. Bessho,T., Sancar,A., Thompson,L.H. and Thelen,M.P. (1997) Reconstitution of human excision nuclease with recombinant XPF-ERCC1 complex. *J. Biol. Chem.*, **272**, 3833–3837.
47. Ichihashi,M., Fujiwara,Y., Uehara,Y. and Matsumoto,A. (1985) A mild form of xeroderma pigmentosum assigned to complementation group G and its repair heterogeneity. *J. Invest. Dermatol.*, **85**, 284–287.
48. Nakano,E., Ono,R., Masaki,T., Takeuchi,S., Takaoka,Y., Maeda,E. and Nishigori,C. (2014) Differences in clinical phenotype among patients with XP complementation group D: 3D structure and ATP-docking of XPD in silico. *J. Invest. Dermatol.*, **134**, 1775–1778.
49. de Weerd-Kastelein,E.A., Keijzer,W. and Bootsma,D. (1974) A third complementation group in xeroderma pigmentosum. *Mutat. Res. - Fundam. Mol. Mech. Mutagen.*, **22**, 87–91.
50. Chavanne,F., Broughton,B.C., Pietra,D., Nardo,T., Browitt,A., Lehmann,A.R. and Stefanini,M. (2000) Mutations in the XPC gene in families with xeroderma pigmentosum and consequences at the cell, protein, and transcript levels. *Cancer Res.*, **60**, 1974–1982.
51. Sethi,M., Haque,S., Fawcett,H., Wing,J.F., Chandler,N., Mohammed,S., Frayling,I.M., Norris,P.G., McGibbon,D., Young,A.R. *et al.* (2016) A distinct genotype of XP complementation group A: Surprisingly mild phenotype highly prevalent in Northern India/Pakistan/Afghanistan. *J. Invest. Dermatol.*, **136**, 869–872.
52. Sidwell,R.U., Sandison,A., Wing,J., Fawcett,H.D., Seet,J.E., Fisher,C., Nardo,T., Stefanini,M., Lehmann,A.R. and Cream,J.J. (2006) A novel mutation in the XPA gene associated with unusually mild clinical features in a patient who developed a spindle cell melanoma. *Br. J. Dermatol.*, **155**, 81–88.
53. Fang,E.F., Scheibye-Knudsen,M., Brace,L.E., Kassahun,H., Sengupta,T., Nilsen,H., Mitchell,J.R., Croteau,D.L. and Bohr,V.A. (2014) Defective mitophagy in XPA via PARP-1 hyperactivation and NAD+/SIRT1 reduction. *Cell*, **157**, 882–896.
54. Godon,C., Mourgues,S., Nonnekens,J., Mourcet,A., Coin,F., Vermeulen,W., Mari,P.-O. and Giglia-Mari,G. (2012) Generation of DNA single-strand displacement by compromised nucleotide excision repair. *EMBO J.*, **31**, 3550–3563.
55. Andressoo,J.-O., Mitchell,J.R., de Wit,J., Hoogstraten,D., Volker,M., Toussaint,W., Speksnijder,E., Beems,R.B., van Steeg,H., Jans,J. *et al.* (2006) An Xpd mouse model for the combined xeroderma pigmentosum/Cockayne syndrome exhibiting both cancer predisposition and segmental progeria. *Cancer Cell*, **10**, 121–132.
56. Fan,L., Fuss,J.O., Cheng,Q.J., Arvai,A.S., Hammel,M., Roberts,V.A., Cooper,P.K. and Tainer,J.A. (2008) XPD helicase structures and activities: insights into the cancer and aging phenotypes from XPD mutations. *Cell*, **133**, 789–800.
57. Fuss,J.O. and Tainer,J.A. (2011) XPB and XPD helicases in TFIIH orchestrate DNA duplex opening and damage verification to coordinate repair with transcription and cell cycle via CAK kinase. *DNA Repair (Amst).*, **10**, 697–713.
58. Moriel-Carretero,M., Herrera-Moyano,E. and Aguilera,A. (2015) A unified model for the molecular basis of Xeroderma pigmentosum -Cockayne Syndrome. *Rare Dis.*, **3**, e1079362.
59. Shiomi,N., Kito,S., Oyama,M., Matsunaga,T., Harada,Y.-N., Ikawa,M., Okabe,M. and Shiomi,T. (2004) Identification of the XPG region that causes the onset of Cockayne syndrome by using Xpg mutant mice generated by the cDNA-mediated knock-in method. *Mol. Cell. Biol.*, **24**, 3712–3719.
60. Ito,S., Kuraoka,I., Chymkowitch,P., Compe,E., Takedachi,A., Ishigami,C., Coin,F., Egly,J.-M. and Tanaka,K. (2007) XPG stabilizes TFIIH, allowing transactivation of nuclear receptors: implications for Cockayne syndrome in XP-G/CS patients. *Mol. Cell*, **26**, 231–243.
61. Trego,K.S., Groesser,T., Davalos,A.R., Parplys,A.C., Zhao,W., Nelson,M.R., Hlaing,A., Shih,B., Rydberg,B., Pluth,J.M. *et al.* (2016) Non-catalytic Roles for XPG with BRCA1 and BRCA2 in Homologous Recombination and Genome Stability. *Mol. Cell*, **61**, 535–546.
62. Le May,N., Fradin,D., Iltis,I., Bougnères,P. and Egly,J.M. (2012) XPG and XPF endonucleases trigger chromatin looping and DNA demethylation for accurate expression of activated genes. *Mol. Cell*, **47**, 622–632.
63. Kamileri,I., Karakasilioti,I., Sideri,A., Kosteas,T., Tatarakis,A., Talianidis,I. and Garinis,G.A. (2012) Defective transcription initiation causes postnatal growth failure in a mouse model of nucleotide excision repair (NER) progeria. *Proc. Natl. Acad. Sci. U.S.A.*, **109**, 2995–3000.
64. Su,Y., Orelli,B., Madireddy,A., Niedernhofer,L.J. and Schärer,O.D. (2012) Multiple DNA binding domains mediate the function of the ERCC1-XPF protein in nucleotide excision repair. *J. Biol. Chem.*, **287**, 21846–21855.